https://erjm.journals.ekb.eg
ISSN: 1110-1180

DOI: ---------

ERJ
Engineering Research Journal
Faculty of Engineering
Menoufia University

Shear Resistance of Haunched and Non-Prismatic Reinforced Concrete Beams

Ahmed F. Elkhouly[1*], Mahmoud Magdy[2], and Boshra A. Eltaly[1]

[1] Civil Engineering Dept., Faculty of Engineering Menoufia University, Egypt.
[2]M. Sc. Candidate, Civil Engineering Dept., Faculty of Engineering Menoufia University, Egypt
*(*Corresponding author: ahmed.elkholy@sh-eng.menofia.edu.eg)*

ABSTRACT
This research is focusing on investigating the influence of tapered and curvature angles on the shear strength of concrete beams. Specifically, the study examined the effect of varying angles in the lower chord and the impact of increasing stirrups on the shear behavior of beams. Seven concrete beams were designed for experimental investigation. One beam was a prismatic with the same cross section along the span, while four beams had different inclination angles of the beam soffit with variable cross section dimensions. The remaining two beams had different stirrup arrangements. All beams were tested under four-point loading and were designed to fail in shear. Additionally, a finite element analysis using ABAQUS 6.14 was conducted to compare the obtained results. The results of the experiments demonstrated a clear link between reducing tapered angles in haunched beams and the enhancement of shear capability. The beams with smaller tapered angles exhibited improved shear strength compared to those with larger angles. Similarly, the incorporation of additional stirrups resulted in an enhancement of the shear capability. The finite element analysis demonstrated a strong correlation in forecasting failure mechanisms with experimental specimens.

Keywords: *RC Beams; Shear Performance; Hunched Beams; Non-prismatic Beams; Finite Element Modeling.*

1. Introduction

Reinforced concrete beams are structural elements characterized by a uniform depth and are susceptible to several forms of stress including bending, shear, and torsion. In contrast, tapered or haunched beams are a distinct category of beams characterized by heterogeneous effective depths along the beam span. The use of beams with haunches not only improves structural efficiency, but also serves as an aesthetic alternative that enables the use of less materials. Additionally, it is imperative to guarantee the presence of enough spatial provisions inside the structure to facilitate the accessibility of mechanical elements such as ducts, pipes, and cables. Simultaneously, it is crucial to implement the necessary formwork and skilled labor to construct the required structures. The use of variable-dimension reinforced concrete (RC) beams is an ideal solution for bridges and high structures, such as overpasses and railway bridges [1-4]. Such beams require different dimensions and diverse reinforcement ratios that significantly impact their structural behavior. Adjusting the ratio of reinforcement used to match the external shape of adjacent structures is necessary, followed by studying the structural behavior of these beams [5,6]. For more than a hundred years, engineers and researchers have struggled to definitively understand the behavior of reinforced concrete elements subjected to shear stresses. The varying effective depth of haunched or tapered elements across their span makes the shear design models in the current codes less effective compared to those available for the design of prismatic beams. Additionally, both prismatic and non-prismatic members differ significantly in failure mechanisms and the analysis of stresses. Arturo et al. [7] examined the demeanor of reinforced concrete haunch beams under static shear loading. Ten types of prototypes simply supported RC beams (eight with haunches and two prismatic) were tested and shown to fail in shear under static stress; the results and interpretations of these tests were presented. Their improved evaluation of the role of inclined longitudinal reinforcement, especially regardless of the amount of moment linked to bond-slip failure, demonstrated its effectiveness for simply supported beams experiencing shear failure. Archundia-Aranda et al. [8] investigated the behavior of RC haunched beams at cyclic shear loading. The outcomes from the cyclic testing approved the validity of a previously suggested empirical equations for assessment. The RC haunched beams shear strength was influenced by different parameters including the angle of the haunch, the shear reinforcement, the concrete compressive strength, and the impact of the inclined longitudinal reinforcement. Domínguez et al.

[9] presented a study on the finite element modeling of reinforced concrete haunched beams that were designed to fail in shear. The research reported and discussed the outcomes of testing eight simply supported beams subjected to static loading in nonlinear finite element models, all designed to fail in shear. Aranda et al. [10] examined the behavior of cyclic RC haunched continuous beams designed to fail in shear. Their research included the testing of five continuous beams (four haunched and one prismatic) under increasing cyclic loading, and the results corroborated previous findings from tests on simply supported beams. Luis et al. [11] investigated the shear strength of RC continuous haunched beams by applying cyclic testing, presenting their research results, interpretations, and findings for five prototype beams designed to fail in shear by applying cyclic loading. Al Jawahery et al. [12] explored the experimental investigation of rehabilitated RC haunched beams using Carbon Fiber Reinforced Polymer (CFRP) strips, supported by 3D finite element modeling analysis. Colunga et al. [13] studied the strengthening of RC prismatic and haunched beams using light jacketing. They presented an experimental study involving eight RC beams (two prismatic and six haunched) that were designed to fail in shear. Majid et al. [14] introduced a new computational optimization model in order to keep the plastic behavior of RC haunched beams by considering the complementary strain energy of residual forces within the reinforcing steel bars. Xin Liu et al. [15] explored the seismic of post-fire performance of RC beam-column joints strengthened by using a steel haunch system. They proposed a practical and creative method for reinforcing fire-damaged RC joints by applying steel haunches. Ziwei Cai et al. [16] investigated the seismic retrofitting of large-scale interior RC beam-column-slab joints after a standard fire exposure, utilizing a steel haunch system to ensure their seismic safety. Mohammad et al. [17] conducted numerical and experimental studies of an innovative shear-resisting steel frame linked to haunched beams, focusing particularly on very short link beams. Albegmprli et al. [18] presented a study that used stochastic and reliability assessments of the ultimate shear capacity of RC haunched beams using nonlinear finite element analysis. The authors demonstrated that compared to RC prismatic beams, RC haunched beams are more sensitive and dangerous. Angela et al. [19] derived an analytical model for non-prismatic beams in 2D according to the Hellinger–Reisner concept, aiming to predict the displacements and stresses in an accurate way. Balduzzi et al. [20] utilized Timoshenko approach to model non-prismatic beams introducing a clear and simple equilibrium, compatibility, and constitutive equations for a non-prismatic planar beam. Yadgar Tayfur et al. [21] studied the ability to optimize non-prismatic concrete beams using a combined-interaction approach, demonstrating that over 40% of concrete may be reduced. Patni et al. [22] focused on efficient modeling of beam-like structures with general non-prismatic, addressing the complexity, curved geometry, and computational expense of analyzing three-dimensional stress states, especially with large deflections causing nonlinear structural responses. Mercuri et al. [23] analyzed non-prismatic beams, discussing accurate stress recovery, critical issues, and the definition of the analytical of the finite element (FE) stiffness matrix, emphasizing their use in strategic of the structures like bridges and sports arenas. Resana et al. [24] assessed the rotation capacity of developed non-prismatic flanged RC T-beams, noting their efficiency in maximizing strength capacity in civil engineering applications. Yang et al. [25] proposed a shear design mechanism for non-prismatic concrete beams reinforced with Wound Fibre-Reinforced Polymer (W-FRP), addressing the challenges of constructing geometrically optimized concrete structures with minimal material consumption using flexible fabric formworks and bespoke W-FRP cages.

2. Aim and Research Significance

This research aims to study the dimensional variations and reinforcement ratios of two types of beams; haunched and non-prismatic, with variable cross sections along the span with the depth increased near the supports. This configuration allows for the traffic needs and enables economic aspects by reducing material usage through structural optimization. The features of each type of beams were analyzed in terms of their ability to withstand shear forces and distribute loads evenly. A numerical model was created to investigate the behavior of these beams that change concrete sections for both types.

3. Experimental Program

3.1. Tested beams and testing procedure

Seven simply supported RC beams were experimentally tested in order to evaluate their shear performance. These beams were divided into three groups as detailed in Table 1. Group 1 comprises one control beam (B0) reinforced with 8 mm diameter steel stirrups spaced at 130 mm intervals along the span, Fig. 1.

Table (1). Configuration and steel reinforcement of test beams

Group	Beam	Beam Type	Inclination Angle, Deg.	Mid-Span Depth, mm	Shear Span Stirrups
G1	B0	Control	0	300	ϕ8@130mm
G2	B-H-6-130	Haunched	6	250	ϕ8@130mm
	B-H-9-130		9	230	ϕ8@130mm
	B-H-6-100		6	250	ϕ8@100mm
G3	B-N-250-130	Non-prismatic	--	250	ϕ8@130mm
	B-N-230-130		--	230	ϕ8@130mm
	B-N-230-100		---	230	ϕ8@100mm

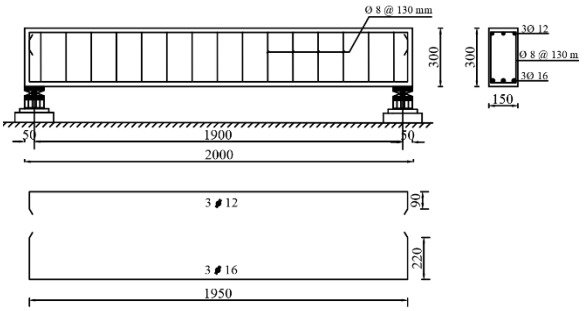

Fig. 1. Geometry and reinforcement details for beam B0 (Dim. in mm)

The control beam had a cross-section of 150 mm × 300 mm, a clear span of 1900 mm, and an overall length of 2000 mm. The beam was reinforced with three 16 mm diameter high tensile steel bars at bottom and three 12 mm diameter compression bars. The beams in the second group were designed to assess the impact of haunches on the shear performance. This group included three beams, the first beam B-H-6-130 (the letter H indicates a haunched beam, the number 6 referred to the inclination angle of the beam soffit, and the number 130 refers to the spacing between stirrups along the shear spans. The other two beams B-H-9-130 and B-H-6-100 were designed to study the influence of the inclination angle and the intensity of shear reinforcement in the shear span as shown in Fig. 2.

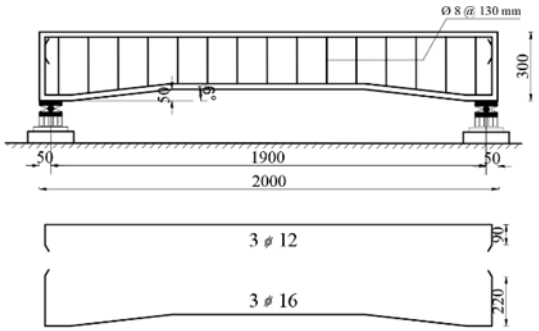

(a)

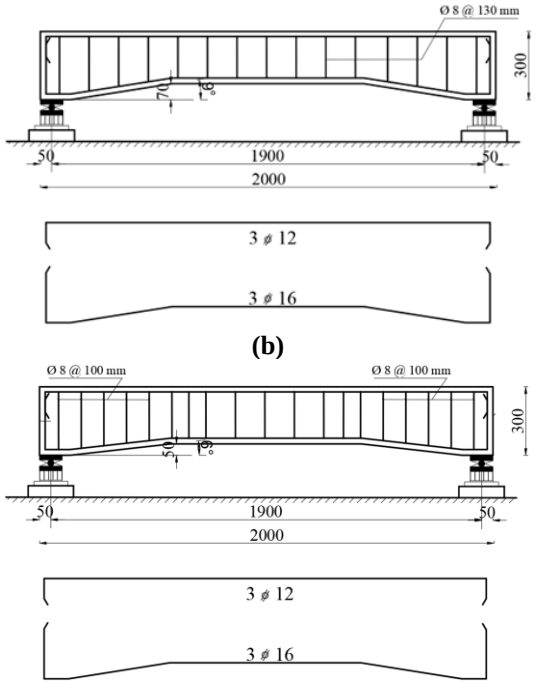

(b)

(c)

Fig. 2. Geometry and reinforcement details of group G2 beams (Dim. in mm)

The third group was intended to study the impact of non-prismatic beams in shear. Three beams were studied herein as reported in Table 1. The first beam B-N-250-130 (the letter N indicates a non-prismatic beam, 250 indicates the beam depth at mid-span, and the number 130 indicated the spacing between stirrups along the shear span. The other two beams, B-N-230-130 and B-N-230-100, were designed to study the influence of beam geometry and shear reinforcement as shown in Fig. 3.

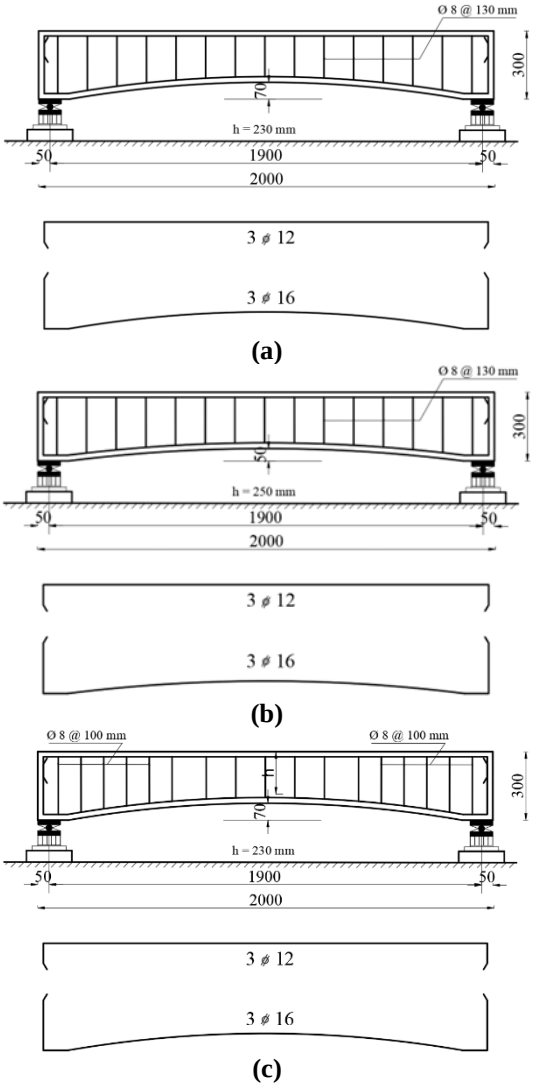

Fig. 3. Geometry and reinforcement details of group G3 beams (Dim. in mm)

3.2. Properties of materials and concrete mix

Table (2) gives concrete mix constituents. The materials included CEM I-42.5 N Portland cement, and crushed dolomite as coarse aggregate with a MNS of 12.5 mm. Standard cylinders (150 mm x 300 mm) were prepared to be tested in compression after 28 days. The average compressive strength was 25.0 MPa. Dog-bone test specimens were used to evaluate the direct tensile strength, Fig. 4(a, b). The tests indicated a brittle behavior under direct tension, as the specimens failed abruptly upon reaching a maximum tensile strength of 3.12 MPa. The stress-strain curves under direct tension and compression are depicted in Fig. 4(c). These curves have been simplified to facilitate numerical modeling. Additionally, the stress-strain attained from the testing the reinforcing rebars along with idealized counterparts, are illustrated in Fig. (5).

Table (2). Concrete mix constituents (kg/m^3)

Cement	Fine aggregate	Coarse aggregate	W/C
350	710	1130	0.42

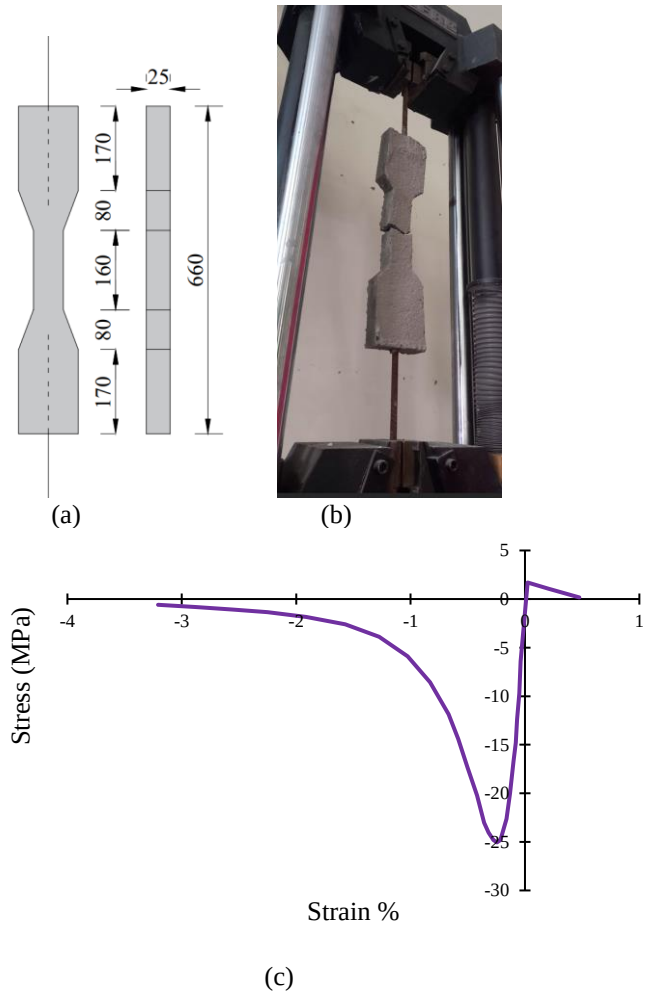

Fig.4. Uniaxial tensile test for concrete: (a) Concrete dimensions, (b) Direct tensile test, and (c) Constitutive compression and tensile stress–strain laws

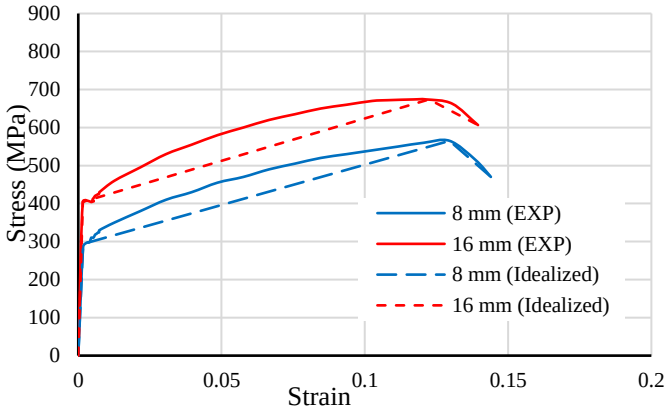

Fig. 5. Experimental and Idealized Tensile Stress-Strain Curves for Reinforcing Steel

3.3. Testing Configuration

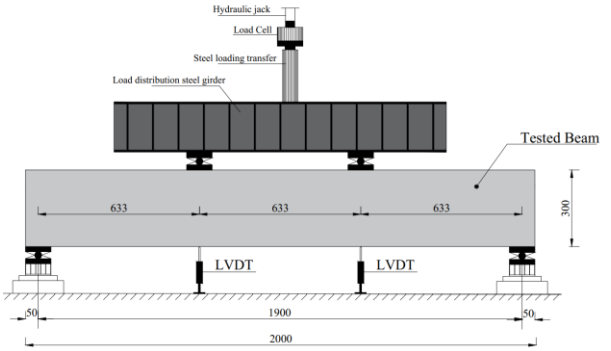

(a)

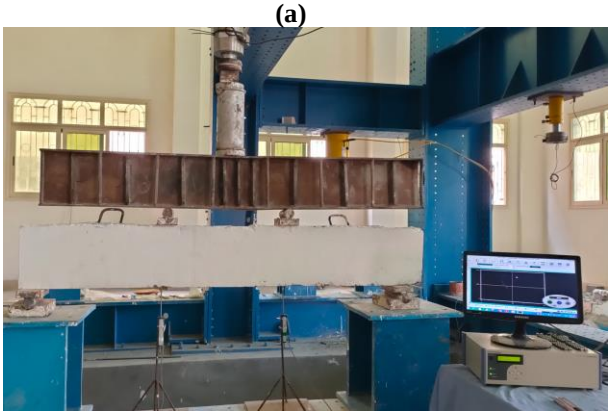

(b)

Fig. 6. Test Setup and Dimensions

Fig. 6 illustrates the configuration of four-point load test. Four rigid supports were used at the supports and loading points for load distribution to avoid localized stresses. The effective span of the beam was 1900 mm, with an overhanging length of 50 mm beyond the supports as shown in Fig. 6. During the test, two LVDTs were installed attached to the beam soffit under the loading points to record the beam deflections. To measure the overall force exerted on the beam under test, a 30000 kN load cell was used. The loads - deflection measurements were recorded using a digital data logger unit and its accompanying software. The beams were loaded till failure through a force control approach.

4. Test Results and Discussion

At this part, discussions are taken to crack patterns, failure modes, load-vertical displacement relationship, elastic index, absorbed energy, and ductility. The experimental results for all haunched, prismatic, and non-prismatic specimens are summarized in Table 3. This table includes data on the cracking load, the associated vertical displacement, ultimate capacity, and maximum deflection.

4.1. Pattern of cracks and shapes of fail

The cracking behavior before failure showed consistent characteristics across all beams until the first fracture occurred. This uniformity is due to the elastic response of all sections to external loads. The initial crack formed in the pure flexural zone as a flexural crack. As the external load increased, additional flexural and shear-flexural cracks developed, with cracks continuing to propagate. Eventually, the initial shear crack emerged in one of the shear spans, and as the loads continued to increase, additional shear cracks developed. However, the propagation of most cracks, except for shear cracks, either stopped or slowed significantly until the beams ultimately failed. Fig. 7 showed the measured crack patterns for the beam tested in Group G1 (B0). The master beam without any changes in cross section, exhibited a classic shear crack pattern and failure mode. Initially, two cracks appeared at the bottom loading positions at 26.5% of the ultimate load (35.95 kN). As the load increased, this crack propagated upwards, while new cracks appeared along the beam span from the supports to the loading plates. Eventually, the number of inclined shear and flexural-shear cracks grew, leading to the beam's failure in shear at 135.22 kN. This beam was designed to serve as the reference for comparison with the haunched and non-prismatic groups.

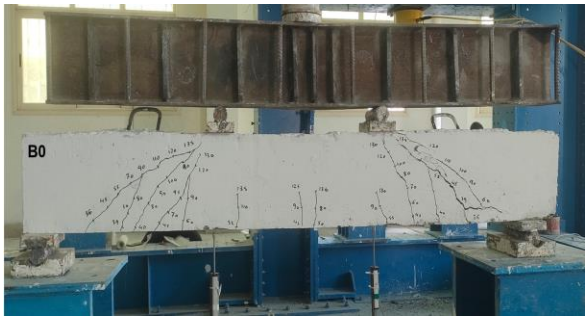

Fig. 7. Failure Mode of The Control Beam B0

The second group that was designed to study the reflection of haunched beams presented a good shear flexural failure mode. Figure 8 shows the crack patterns observed in haunched beams from the second group (group G2). It is clear that the lower inclination angle in these beams improved crack distribution and compensated for the tested beams. Frist cracks initiated at critical loads of approximately 22.47 kN, 20.03 kN, and 32.76 kN for beams B-H-6-130, B-H-9-130, and B-H-6-100, respectively. At the higher inclination angle, more cracks generated rapidly at shear zone. In such haunched beams, most remarkable cracks were formed in the shear zone with diagonal appearance. At load levels between 70-85% of the ultimate capacity, more diagonal cracks widened and

continued to grow until failure. Increasing the load to 90% of PU resulted in denser cracks shifting towards the middle zone. Additionally, increasing the amount of steel stirrups in the outer third led to the appearance of flexural cracks due to stress concentration, as demonstrated in Fig. 8(c).

It is important to note that only one wide inclined crack shifted horizontally near the concrete cover, with an inclination angle of 9 degrees. Ultimately, the tested beams were unable to absorb any additional load once concrete crushing occurred. The ultimate capacity of the tested beams in the second group was recorded. as P_u= 105.67 kN, 85.36 kN, and 128.39 kN for beams B-H-6-130, B-H-9-130, and B-H-6-100, respectively as presented in Table 3.

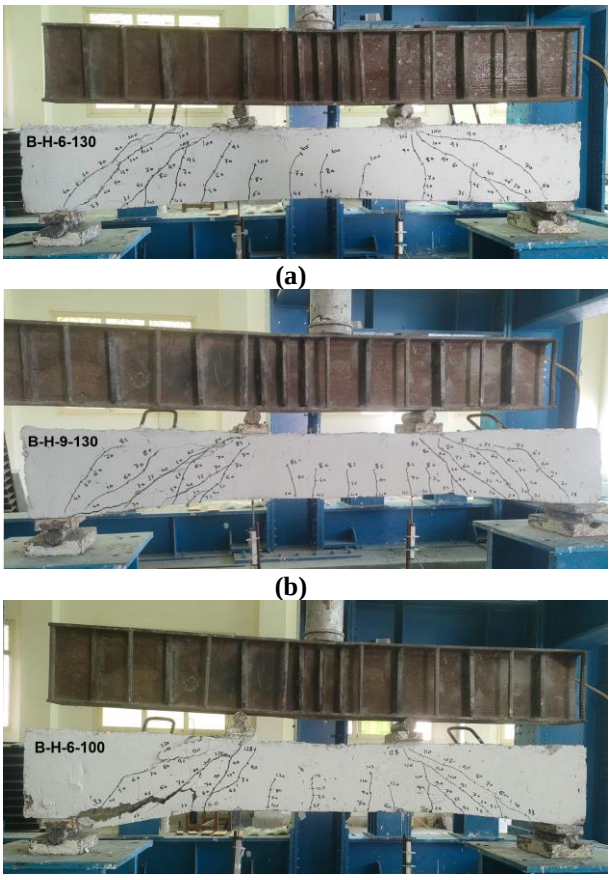

Fig. 8. Failure Mode of Group G2 Beams

The third group was prepared to investigate the impact of non-prismatic beams. These beams exhibited a favorable shear-flexural failure mode, as shown in Fig. 9. The crack patterns observed in these non-prismatic beams were examined in the third group (G3). It is worth noting that the curved surface on the lower side of the tested beam increased the cracking loads compared to the previous group (haunched beams) with the same mid-span depth, as summarized in Table 3. Frist cracks initiated at loading location of approximately 29.56 kN, 22.47 kN, and 35.27 kN for beams B-N-250-130, B-N-230-130, and B-N-230-100, respectively as presented in Table 3. These beams captured 82%, 63%, and 98% of PU of the master beam. At the smaller depth, shear cracks clearly appeared at the shear zone in the outer third. In such non-prismatic beams, most shear cracks were formed in the shear zone with diagonal feature. At load level ranged in between 75-88% of ultimate capacity, more diagonal cracks became wider and continued to enlarger up to collapse. When the spacing between the used steel stirrups in the outer third led to the appearance of small flexural cracks, as depicted in Fig. 8(c). The beam B-N-250-100 gained the best configuration of such type of beams. At the ultimate stage, the tested beams could not sustain any additional load when concrete crushing occurred at the loading location. The ultimate capacities of the tested beams in the second group were recorded as Pu = 118.46 kN, 92.89 kN, and 131.45 kN for beams B-N-250-130, B-N-230-130, and B-N-230-100, respectively, as shown in Table 3.

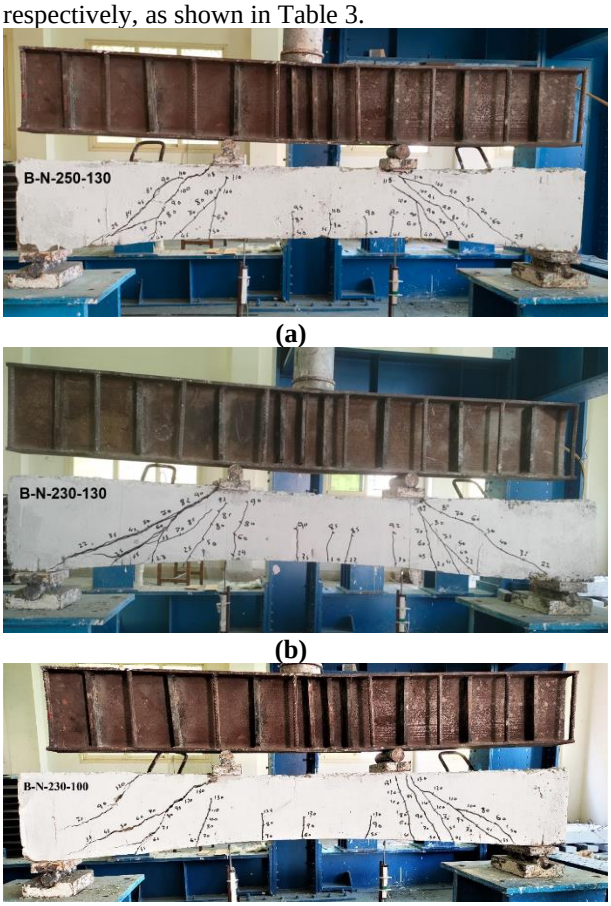

Fig. 9. Failure Mode of Group G3 Beams.

4.2. Load deflection relationship, absorbed energy, elastic index, and ductility

Fig. 10 presents the typical shear load-deflection relationship captured for all tested beams. That relationship can be divided into four distinct phases. The first phase is elastic, where the beam behaves as a perfectly elastic member and does not exhibit any significant cracks. Deformations are minimal and fully recoverable once the load is removed. The cracking phase starts with the appearance of the first crack, causing the load-deflection relationship to deviate from linearity as the beam's stiffness decreases due to crack formation and growth. As the load increases, the steel reinforcement eventually yields in the yielding stage, making the curve steeper due to a further reduction in stiffness. Ultimately, the beam reaches its maximum capacity and fails, unable to support the applied load during the failure stage.

Initially, Beam B0 displayed a linear response during the elastic phase. Cracking began at 35.95 kN, causing a gradual decrease in stiffness while still maintaining linearity until around 85 kN. Subsequently, yielding occurred, initiating the nonlinear phase of the curve, which continued until reaching the maximum load of 135.22 kN, at which point shear failure became apparent presented in Fig. 10(a). The use of haunched beams in Group G2 resulted in a performance shortfall compared to B0 and could not match the behavior of the reference specimen B0. Increasing the inclination angle of the lower surface led to reduced elastic stiffness, cracking load, and ultimate load, thereby offering lower deformation capacity. Using 6° and 9° angles resulted in respective increases of 69% and 50% in elastic stiffness (see Fig. 11(b)), 63% and 56% in cracking load, and 78% and 63% in ultimate load for beams B-H-6-130 and B-H-9-130, respectively. Additionally, the ductility and absorbed energy for these beams were recorded as indicators of the plastic stage range preferred in construction. The beam B-H-6-100, with 100 mm spacing, showed significant contributions to both cracking and ultimate loads, achieving 91% and 95% of the cracking and ultimate loads of the master beam, respectively, as summarized in Table 3. Application of curved surface in the non-prismatic beams in third group substantially improved the load-deflection performance. The increase in depth at mid span hindered the propagation of inclined cracks, delaying failure and enhancing beam capacity. Compared to haunched beams, the introduction of curved surface led to significant improvements, with crack load increments of 82%, 63%, and 98% for B-N-250-130, B-N-230-130, and B-N-230-100, respectively. Correspondingly, there were noticeable increases of 88%, 69%, and 97% in ultimate load, along with enhancements of approximately 66%, 52%, and 119% in elastic stiffness, as detailed in Table 3

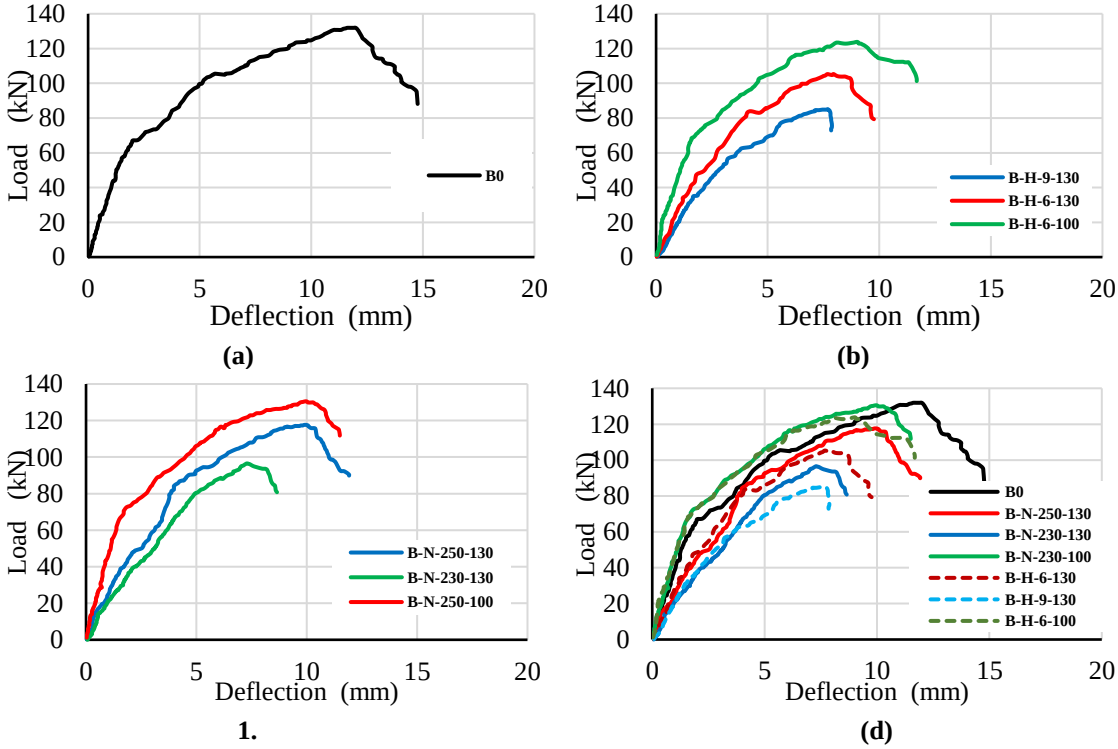

Fig. 10. Load-deflection relationships for tested beams: (a) Master beam, (b) Group G2, (c) Group G3, and (d) All specimens.

Table (3): Test Results of The Tested Beams.

	Specimen`s ID	Cracking Stage			Ultimate Stage			Elastic Stiffness Index (K)	K_B/K_{DB}	Absorbed Energy (E)	E_B/E_{DB}	Ductility
		P_{cr} (kN)	P_{crB}/P_{crB0}	Δ_{cr} (mm)	P_u (kN)	P_{uB}/P_{uB0}	Δ_{Pu} (mm)					
G1	**B0**	35.95	1.00	0.91	135.22	1.00	11.99	39.46	1.00	1450.83	1.00	13.16
G2	**B-H-6-130**	22.47	0.63	0.83	105.67	0.78	7.93	27.07	0.69	727.26	0.50	9.55
	B-H-9-130	20.03	0.56	1.02	85.36	0.63	7.69	19.70	0.50	436.47	0.30	7.56
	B-H-6-100	32.76	0.91	0.63	128.39	0.95	9.04	52.17	1.32	1132.38	0.78	14.39
G3	**B-N-250-130**	29.56	0.82	1.13	118.46	0.88	10.05	26.16	0.66	993.50	0.68	8.89
	B-N-230-130	22.47	0.63	1.10	92.89	0.69	7.39	20.41	0.52	540.53	0.37	6.71
	B-N-230-100	35.27	0.98	0.75	131.45	0.97	10.01	47.15	1.19	1151.60	0.79	13.38

P_{cr}: Load at which the first crack appeared; **Δ_{cr}**: Vertical deflection recorded at P_{cr}; **P_u**: Ultimate load; **Δ_{Pu}**: Vertical deflection recorded at P_U; **K**: elastic index; **E**: Absorbed energy.

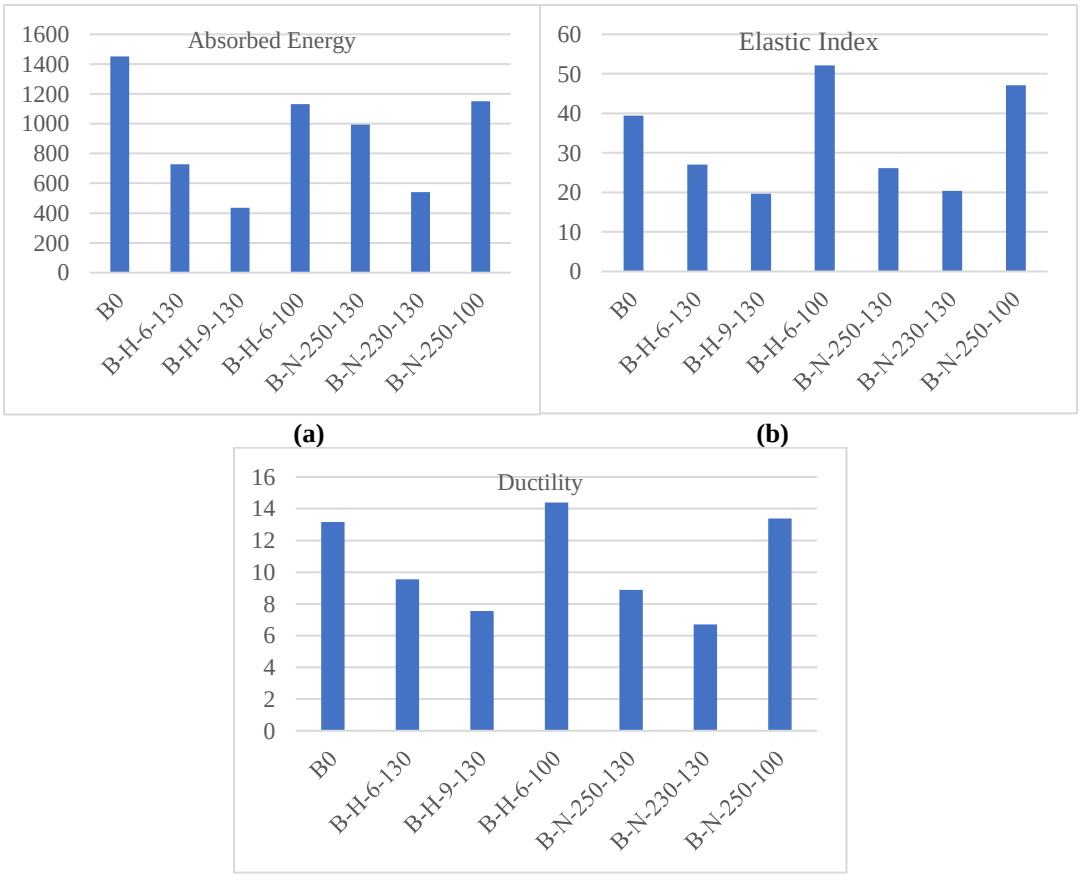

Fig. 11. Experimental outcomes for all tested beams: (a) Absorbed energy (units: kN.mm), (b) Elastic index (units: kN/mm), and (c) Ductility.

5. Numerical Simulation

5.1. Materials Modeling and Analysis

The ABAQUS software was used to model tested beams, and the Concrete Damage Plasticity (CDP) model was used to simulate the behavior of the concrete as recommended previously [26-31]. The plastic damage models developed by Lubliner et al. were utilized to represent the plastic behavior of concrete, while the stress-strain relationship identified by Carreira and Chu was employed to model compressed concrete. The constitutive parameters of the CDP model for ordinary concrete were fine-tuned through multiple iterations. The parameters were adjusted iteratively until a satisfactory match between the simulated stress-strain behavior and the experimental data was achieved. The stress-strain relationship depicted in Figure 4 was used as a reference for validating the accuracy of the simulated results. Significant efforts were undertaken to determine the optimal values for the constitutive parameters used in the Concrete Damage Plasticity (CDP) model for normal concrete. These includes the viscosity relaxation parameter (μ), which varied between 0.0 and 0.001, and the angle of dilation (ψ), suggested by researchers to be 35. The eccentricity (e) was set at 0.1 as suggested by the software, while the ratio of the second stress invariant on the tensile to compressive meridian (Kc) typically ranged from 0.64 to 0.80. The ratio of biaxial to uniaxial compressive yield stresses (fbo/fco) was found to be between 1.10 and 1.16 in previous studies, with 1.16 being used in this investigation. Two types of high tensile steel bars, with diameters of 16 mm and 12 mm, were used as the primary reinforcement in the concrete structures, as shown in Fig. 4(a). Additionally, 8 mm diameter mild steel bars were used as stirrups.

5.2. Finite Element Model Innovation

A nonlinear Finite Element (FE) model was developed to emulate the behavior of RC beams subjected to static monotonic loading until failure. The RC beams were meshed using the continuum, three-dimensional unit cell with eight-node linear hexahedral solid element with reduced integration (C3D8R) accessible inside the ABAQUS software, as illustrated in Figure 12(a). The steel bars were modeled taking two-node linear truss elements (T3D2), as shown in Figure 12(b). Thick loading plate, characterized by higher stiffness, was also meshed using the C3D8R element. The beam was set with a simply supported boundary condition. The loading and boundary conditions used in the FE model are depicted in Figure 12(c). The developed model, with a mesh size of approximately 100 mm, demonstrated satisfactory performance with reduced computational cost. Figure 12 shows the mesh taken in the developed FE model.

In the FE model, a perfect bond interaction between concrete and steel reinforcement was assumed, using the embedded element mechanism available in ABAQUS. This approach involved designating the concrete beam as the host region, with the steel bar truss elements identified as the embedded elements.

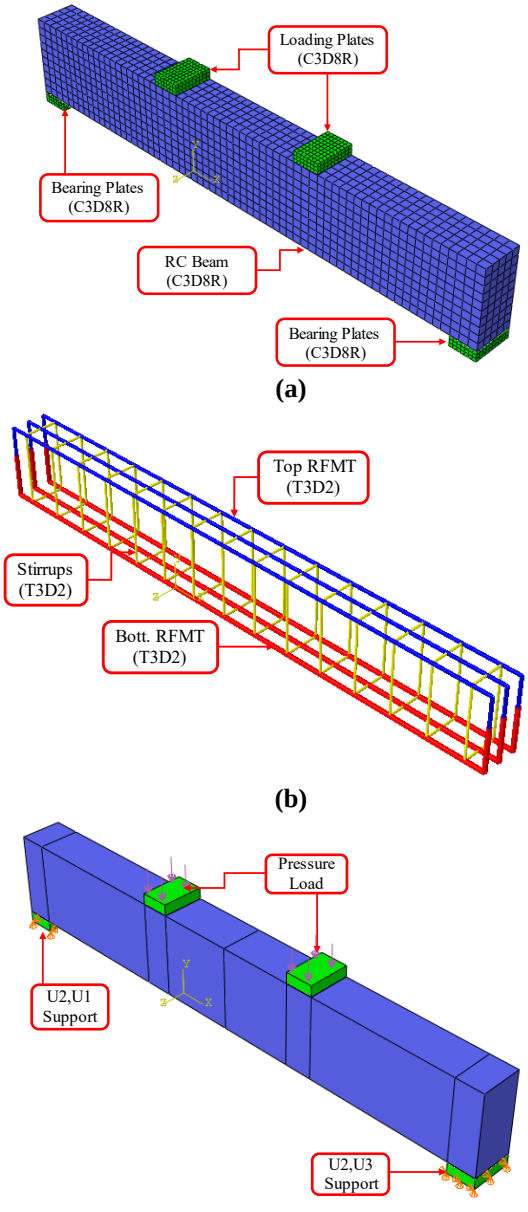

Fig. 12. Finite element model: (a) Concrete elements, (b) reinforcement elements, and (c) Loading and boundary conditions.

5.3. Finite Element Model Verification

To evaluate the accuracy of the developed FE model, a comparison was made between the numerical simulations and the experimental data. This comparison focused on load-deflection response, failure mechanisms, cracking, and ultimate load capacities. The load-displacement results from the numerical simulations were compared with the experimental findings, as shown in Figure 13. Additionally, Table 4 presents the cracking and ultimate loads from both experimental and numerical analyses. The primary failure modes predicted by the FE model are illustrated in Figure 14. From Figure 13, it is evident that the finite element model accurately reproduces the experimentally obtained load-deflection curves of the beams.

Table (4): Finite element and experimental results.

Specimen ID	P_{cr} (kN)		P_u (kN)	
	EX	FE	EX	FE
B0	35.95	32.67	135.22	118.34
B-H-9-130	22.47	21.28	105.67	95.42
B-H-6-130	20.03	24.12	85.36	84.11
B-H-6-100	32.76	34.09	128.39	104.20
B-N-250-130	29.56	32.67	118.46	98.64
B-N-230-130	22.47	21.28	92.89	84.21
B-N-230-100	35.27	34.81	131.45	128.51

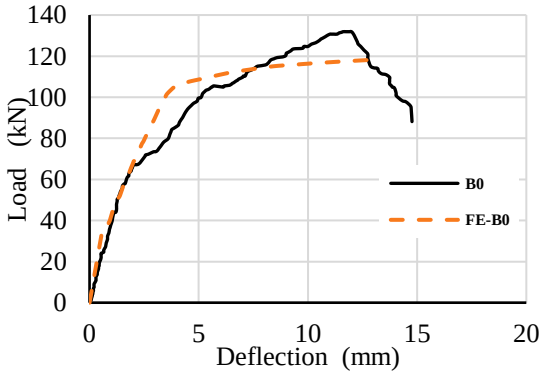

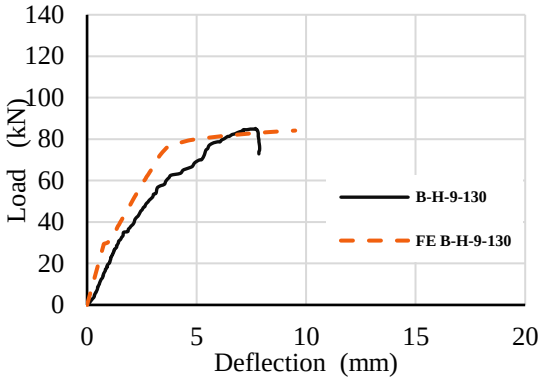

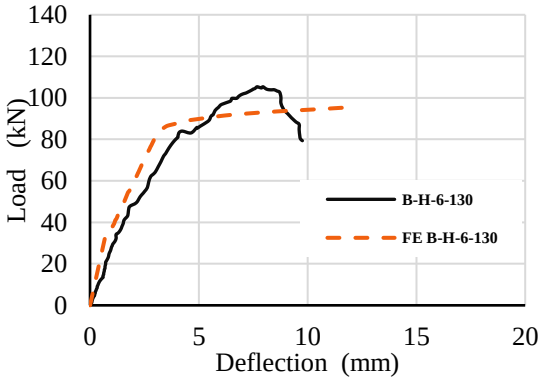

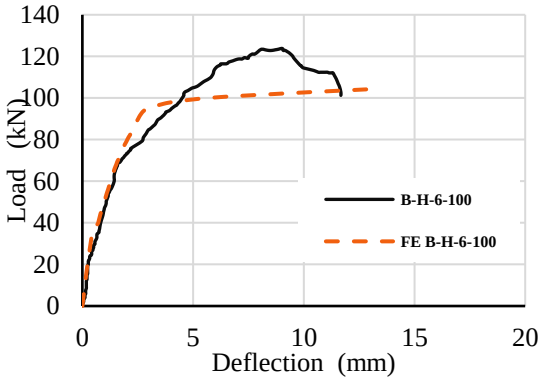

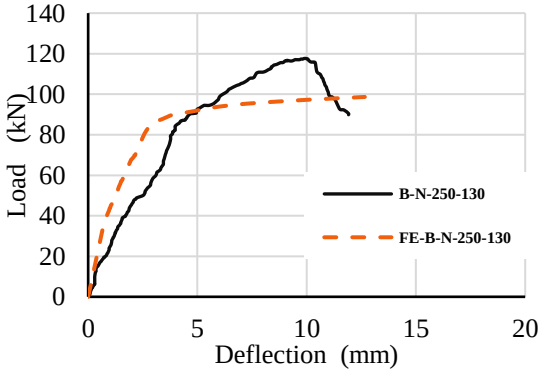

Fig. 13. Load deflection curves for experimental and FE under load for all specimens.

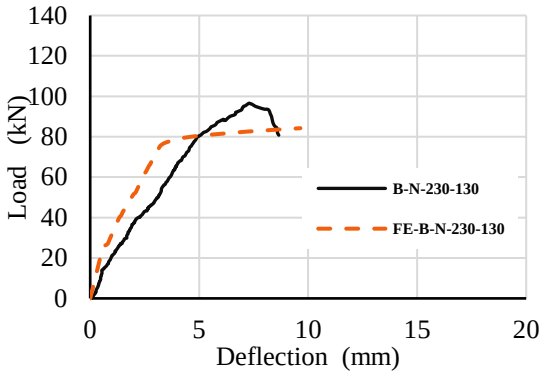

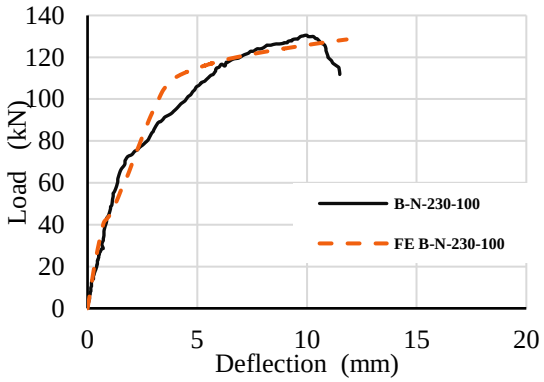

Fig. 13-continued. Load deflection curves for experimental and FE under load for all specimens.

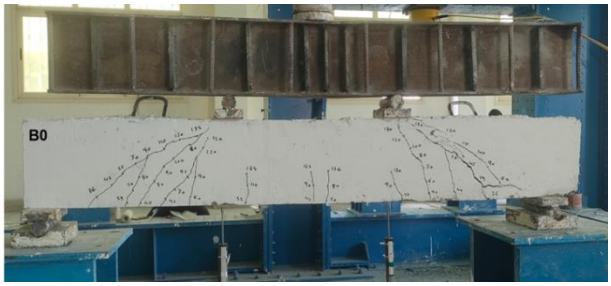

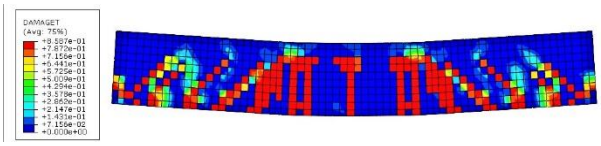

(a) B0 specimen

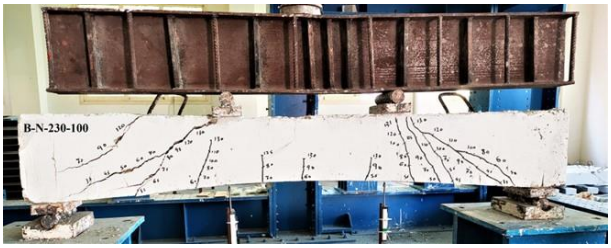

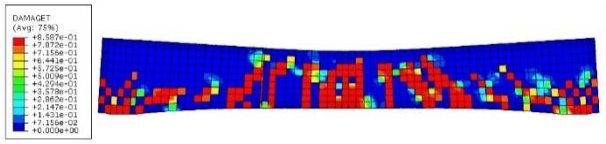

(b) B-N-230-100 specimen

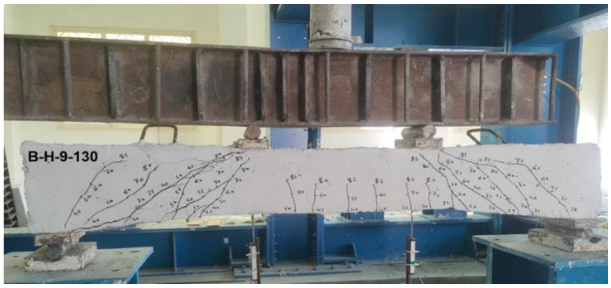

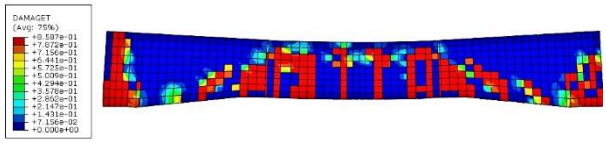

(c) B-H-9-130 specimen

Fig. 14. Verification of crack pattern between FE and Experimental.

As presented in Table 4, the cracking and ultimate loads of the tested beams are accurately expected by the FE model. The average value of $P_{cr\ FE}/P_{cr\ EXP}$ ratios is 1.02. The average ratio of $P_{U\ FE}$ to $P_{U\ EXP}$ is 0.90. The anticipated failure mode is analyzed in conjunction with the test results presented on Fig. 14. The model validation is evident in the softening behavior observed in the load–deflection response illustrated in Fig. 14. The figure illustrates that the finite element model accurately represents the failure shape of the tested beams. The FE model indicates that the principal fracture originated at the bottom of the mid-span at maximum moments, propagated to the shear zone, and extended to the top surface, as evidenced by the test.

6. Parametric study

Building on the successful use of haunched and non-prismatic configurations, a detailed parametric analysis was performed to investigate the impact of using 10 mm steel bars as stirrups for both haunched and non-prismatic beams. As shown in Table 5, the study examines how changes in the lower surface inclination angle for haunched beams and the effective depth for non-prismatic beams influence the load-bearing capacity of the beams at both the cracking and ultimate stages.

Table (5): Test matrix for models studied in the parametric study.

Gro.	Beam ID	Beam Type	Inclination angle (q)	Mid span high (h)	Distribution of stirrups	Main stirrups	Stirrups in the outer third
Haunched beam with 10 mm uniformly distributed stirrups							
G1	H-6-130	Haunched beam	6^O	250 mm	Uniform	ϕ10@130mm	ϕ10@130mm
	H-9-130		9^O	230 mm			
	H-12-130		12^O	210 mm			
Haunched beam with 10 mm ununiformly distributed stirrups							
G2	H-6-100	Haunched beam	6^O	250 mm	Nonuniform	ϕ10@130mm	ϕ10@100mm
	H-9-100		9^O	230 mm			
	H-12-100		12^O	210 mm			
Non-prismatic beam with 10 mm uniformly distributed stirrups							
G3	N-250-130	Non-prismatic beam	----------	250 mm	Uniform	ϕ10@130mm	ϕ10@130mm
	N-230-130		----------	230 mm			
	N-210-130		----------	210 mm			
Non-prismatic beam with 10 mm nonuniformly distributed stirrups							
G4	N-250-100	Non-prismatic beam	----------	250 mm	Nonuniform	ϕ10@130mm	ϕ10@100mm
	N-230-100		----------	230 mm			
	N-210-100		----------	210 mm			

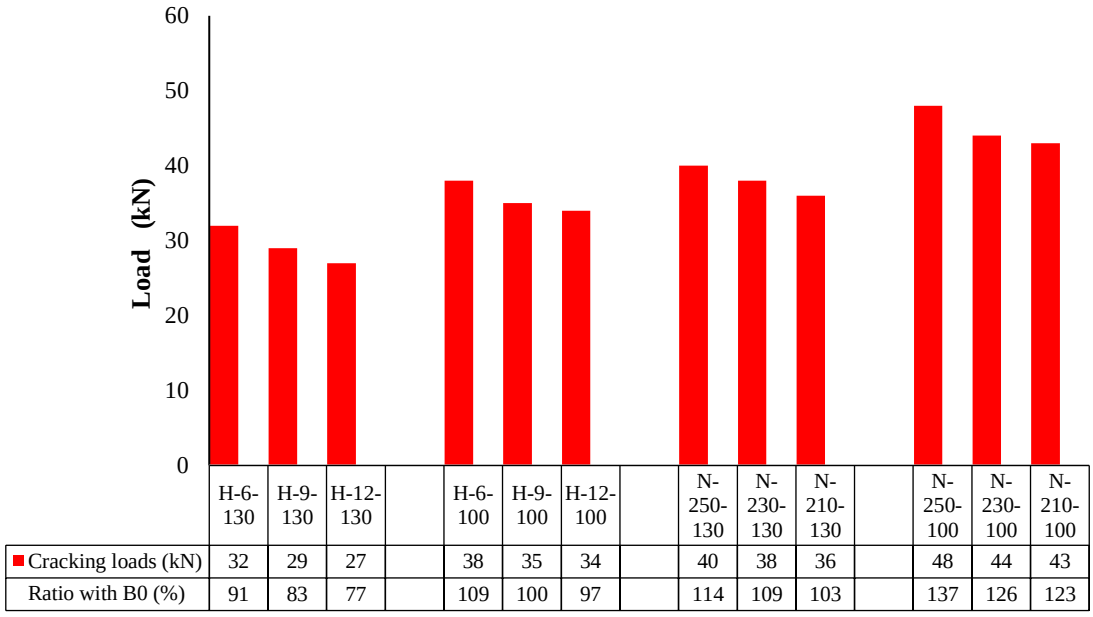

Fig. 15. Parametric study outcome in cracking stage.

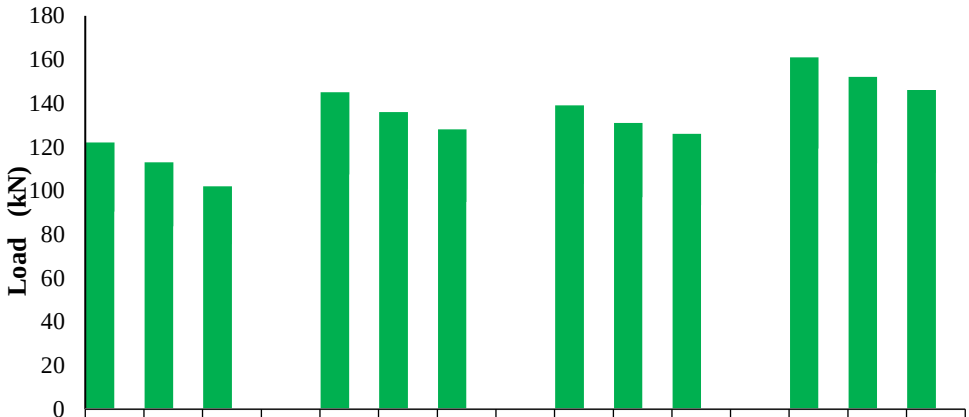

	H-6-130	H-9-130	H-12-130		H-6-100	H-9-100	H-12-100		N-250-130	N-230-130	N-210-130		N-250-100	N-230-100	N-210-100
Ultimate loads (kN)	122	113	102		145	136	128		139	131	126		161	152	146
Ratio with B0 (%)	90	84	76		107	101	95		103	97	93		119	113	108

Fig. 16. Parametric study outcome in ultimate stage.

As presented in Table 5, the first and second group were designed to evaluate the shear performance of RC haunched beams. Each group consisted of three beams. The inclination angles of the lower surface at the outer third for tested beams were 6º, 9º, and 12º for beams H-6-130, H-9-130, and H-12-130, respectively. The first group aimed to study the beams having uniform stirrups distribution with 130 mm spacing. The second group was designed to investigate the beams having nonuniform stirrups distribution with 130 mm spacing in the middle span and 100 mm spacing for the outer third. In the other side the third and fourth group were taken to assess the reflection of 10 mm steel stirrups on the shear performance of non-prismatic beams. Three mid span depths were studied herein those were: 250 mm, 230 mm, and 210 mm. Theses depths were studied in both third and fourth group but the stirrups in the third group distributed uniformly and nonuniformly in the fourth one as summarized in Table 5.

6.1. Impact of beams configuration

All the results indicated that the non-prismatic beams are more effective than its counterparts in haunched beams. The non-prismatic beams enhanced the cracking loads by about 3% - 37% and improved the total ultimate capacity by about 19% higher than the master beam (B0) as shown in Figs. 15 and 16. It is worth noting that increasing the inclination angle of the lower surface of these beams reduced their ultimate capacity, even with the same reinforcement ratio. For haunched beams, the loads decreased by approximately 10% to 24% compared to the master beam. Additionally, the reduction in non-prismatic beams ranged from 3% to 7%, as shown in Fig. 15. The greater contribution of the arched surface on the lower side is highlighted here. In this context, non-prismatic beams demonstrated better load transfer capabilities than haunched beams.

6.2. Impact of stirrups distribution

The results also showed that using 10 mm steel stirrups can effectively restore the ultimate capacity of haunched and non-prismatic beams. The application of 10 mm steel bars as shear reinforcement increased the cracking loads by approximately 14% and 37% for uniformly and non-uniformly non-prismatic beams, respectively. Additionally, the ultimate capacities were improved by about 3% and 19%, as illustrated in Fig. 16.

7. Conclusions

The current research presents investigations of the shear performance of reinforced concrete beams with varied depths, including tapered and curved beams. The augmentation of tapering angles or curvature results in an escalation of cracks and fracture propagation due to heightened flexural stress at the mid-span of the beams. The incorporation of stirrups in tapered or curved beams enhances shear performance by redistributing stress at crack locations through the stirrup legs. A nonlinear finite element model of the beams was created using ABAQUS and validated against experimental data. Conclusions were drawn from both experimental and numerical studies as follows:

1. Using curvature enhanced the shear behavior of the beam more than using tapered section with the same properties as with about 9% as the tapered angel causes stress concentration.
2. Increasing the number of stirrups in tapered or curved sections significantly impacted the shear strength of the beams, with the failure load increasing by 22% and 42%, respectively.
3. The proposed finite element model accurately predicted the structural behavior of reinforced concrete tapered and curved beams. Therefore, this finite element model can be used for future parametric analyses.

8. References:

[1] Su, J., Li, Z. X., Dhakal, R. P., Li, C., & Wang, F. (2021, February). Comparative study on seismic vulnerability of RC bridge piers reinforced with normal and high-strength steel bars. In *Structures* (Vol. 29, pp. 1562-1581). Elsevier.

[2] El Zareef, M. A., Ghalla, M., Hu, J. W., & El-Demerdash, W. E. (2024). Damage detection of lightweight concrete dual systems reinforced with GFRP bars considering various building heights and earthquake intensities. Case Studies in Construction Materials, 20, e03191.

[3] Emara, M., Ghalla, M., Hu, J. W., Badawi, M., Mlybari, E. A., & Ahmed, S. O. (2024). Enhancement of cantilevered RC beams exhibiting inadequate lap spliced reinforcement using sustainable reinforced ECC layers. Construction and Building Materials, 428, 136272.

[4] A. F. Elkhouly, A. Nabil, N. N. Meleka (2020). A State-Of-The-Art Review on Strengthening Of Reinforced Concrete Slabs With Openings. Al-Azhar University Civil Engineering Research Magazine, Vol.42(3) 127-141

[5] El-Taly, B., Hamdy, M., Kandil, K., & Bashandy, A. (2021). Structural Behavior of Strengthened Concrete-Encased Steel Beams with Web Openings. International Journal of Civil Engineering, 19(3), 245-263.

[6] Ghalla, M., Bahrami, A., Badawi, M., & Mlybari, E. A. (2024). Novel sustainable techniques for enhancing shear strength of RC beams mitigating construction failure risk. Ain Shams Engineering Journal, 103017.

[7] Tena-Colunga, A., Archundia-Aranda, H. I., & González-Cuevas, Ó. M. (2008). Behavior of reinforced concrete haunched beams subjected to static shear loading. Engineering Structures, 30(2), 478-492.

[8] Archundia-Aranda, H. I., Tena-Colunga, A., & Grande-Vega, A. (2013). Behavior of reinforced concrete haunched beams subjected to cyclic shear loading. Engineering Structures, 49, 27-42.

[9] Godínez-Domínguez, E. A., Tena-Colunga, A., & Juárez-Luna, G. (2015). Nonlinear finite element modeling of reinforced concrete haunched beams designed to develop a shear failure. Engineering Structures, 105, 99-122.

[10] Tena-Colunga, A., Urbina-Californias, L. A., & Archundia-Aranda, H. I. (2017). Cyclic behavior of continuous reinforced concrete haunched beams with transverse reinforcement designed to fail in shear. Construction and Building Materials, 151, 546-562.

[11] Tena-Colunga, A., Urbina-Californias, L. A., & Archundia-Aranda, H. I. (2017). Assessment of the shear strength of continuous reinforced concrete haunched beams based upon cyclic testing. Journal of Building Engineering, 11, 187-204.

[12] Al Jawahery, M. S., Gulsan, M. E., Albegmprli, H. M., Mansoori, I. A. H., & Cevik, A. (2019). Experimental investigation of rehabilitated RC haunched beams via CFRP with 3D-FE modeling analysis. Engineering Structures, 196, 109301.

[13] Al Jawahery, M. S., Gulsan, M. E., Albegmprli, H. M., Mansoori, I. A. H., & Cevik, A. (2019). Experimental investigation of rehabilitated RC haunched beams via CFRP with 3D-FE modeling analysis. Engineering Structures, 196, 109301.

[14] Rad, M. M., Ibrahim, S. K., & Lógó, J. (2022, May). Limit design of reinforced concrete haunched beams by the control of the residual plastic deformation. In Structures (Vol. 39, pp. 987-996). Elsevier.

[15] Liu, X., Gernay, T., Li, L. Z., & Lu, Z. D. (2021). Seismic performance of post-fire reinforced concrete beam-column joints strengthened with steel haunch system. Engineering Structures, 234, 111978.

[16] Cai, Z., Liu, X., Wu, R., Li, L., Lu, Z., & Yu, K. (2022). Seismic retrofit of large-scale interior RC beam-column-slab joints after standard fire using steel haunch system. Engineering Structures, 252, 113585.

[17] Rahnemoun, M., Tabrizi, S. K., & Ashtari, P. (2022). Experimental and numerical study on innovated steel Shear Resisting Frame with Haunched Beams (SRFHBs). Journal of Constructional Steel Research, 197, 107495.

[18] Albegmprli HM, Çevik A, Gülsan ME, Kurtoglu AE (2015). Reliability analysis of reinforced concrete haunched beams shear capacity based on stochastic nonlinear FE analysis. Comput Concr;15(2):259–77..

[19] Beltempo, A., Balduzzi, G., Alfano, G., & Auricchio, F. (2015). Analytical derivation of a general 2D non-prismatic beam model based on the Hellinger–Reissner principle. Engineering Structures, 101, 88-98.
[20] Balduzzi, G., Aminbaghai, M., Sacco, E., Füssl, J., Eberhardsteiner, J., & Auricchio, F. (2016). Non-prismatic beams: a simple and effective Timoshenko-like model. International Journal of Solids and Structures, 90, 236-250.
[21] Tayfur, Y., Darby, A., Ibell, T., Orr, J., & Evernden, M. (2019). Serviceability of non-prismatic concrete beams: Combined-interaction method. Engineering Structures, 191, 766-774.
[22] Patni, M., Minera, S., Weaver, P. M., & Pirrera, A. (2020). Efficient modelling of beam-like structures with general non-prismatic, curved geometry. Computers & Structures, 240, 106339.
[23] Mercuri, V., Balduzzi, G., Asprone, D., & Auricchio, F. (2020). Structural analysis of non-prismatic beams: Critical issues, accurate stress recovery, and analytical definition of the Finite Element (FE) stiffness matrix. Engineering Structures, 213, 110252.
[24] Zamel, J. K. (2021). Rotation capacity assessment in developed non prismatic flanged reinforced concrete Tee beams. Case Studies in Construction Materials, 14, e00517.
[25] Yang, Y., Shu, J., Zhao, W., & Orr, J. (2021, April). Shear design method for non-prismatic concrete beams reinforced using W-FRP. In Structures (Vol. 30, pp. 667-677). Elsevier.
[26] Ghalla, M., Badawi, M., Elsamak, G., Ahmed, M., Liang, Q. Q., & El Zareef, M. A. (2024). Strengthening of reinforced concrete beams with insufficient lapped splice length of reinforcing bars. Engineering Structures, 321, 118922.
[27] Ghalla, M., Mansour, W., Li, W., Wang, P., Badawi, M., & El Zareef, M. A. (2024). Enhancing the punching performance of two-way RC flat slabs using different configurations of embedded aluminum sections: Experimental program and numerical analysis. Construction and Building Materials, 434, 136737.
[28] El Zareef, M. A., Ghalla, M., Hu, J. W., & El-Demerdash, W. E. (2024). Damage detection of lightweight concrete dual systems reinforced with GFRP bars considering various building heights and earthquake intensities. Case Studies in Construction Materials, 20, e03191.
[29] Ghalla, M., Badawi, M., Mlybari, E. A., & Hu, J. W. (2024). Enhancing shear strength of RC beams through externally bonded reinforcement with stainless-steel strips and FRCM jacket to mitigate the failure risk. Results in Engineering, 22, 102246.
[30] Alharthai, M., Bahrami, A., Badawi, M., Ghalla, M., Elsamak, G., & Abdelmgeed, F. A. (2024). Numerical study on enhancing shear performance of RC beams with external aluminum alloy plates bonded using steel anchors. Results in Engineering, 22, 102143.
[31] Emara, M., Ghalla, M., Hu, J. W., Badawi, M., Mlybari, E. A., & Ahmed, S. O. (2024). Enhancement of cantilevered RC beams exhibiting inadequate lap spliced reinforcement using sustainable reinforced ECC layers. Construction and Building Materials, 428, 136272.